High-Power Performance of a 100-kW Class Nested Hall Thruster

IEPC-2017-228

Presented at the 35th International Electric Propulsion Conference
Georgia Institute of Technology – Atlanta, Georgia – USA
October 8–12, 2017

Scott J. Hall,* Benjamin A. Jorns,† and Alec D. Gallimore‡
University of Michigan, Ann Arbor, MI, 48109, USA

Hani Kamhawi,§ Thomas W. Haag,¶ and Jonathan A. Mackey,‖
NASA Glenn Research Center, Cleveland, OH, 44135, USA

James H. Gilland**
Ohio Aerospace Institute, Brookpark, OH, 44142, USA

Peter Y. Peterson††
Vantage Partners, NASA Glenn Research Center, Cleveland, OH, 44135, USA

and

Matthew J. Baird‡‡
Western Michigan University, Kalamazoo, MI, 49008, USA

The performance of a three-channel, 100-kW class nested Hall thruster was evaluated on xenon propellant for total powers up to 102 kW at NASA Glenn Research Center. The thruster demonstrated stable operation in all seven available channel combinations at discharge voltages from 300 V to 500 V and three different current densities. The resulting test matrix contained forty-six unique conditions ranging from 5 to 102 kW total power and 16 to 247 A discharge current. At each operating condition, thruster performance was measured, and from these measurements specific impulse and efficiency were calculated. All seven channel combinations showed similar performance at a given discharge voltage and current density. The largest thrust recorded was 5.4 N ± 0.1 N at 99 kW, 400 V discharge voltage. Total efficiency and specific impulse ranged from 0.54 to 0.67 ± 0.03 and 1800 seconds to 2650 seconds ± 60 seconds, respectively. It was found that the thrust of the three channels firing together was not larger than the sum of each channel firing individually. Discharge current oscillations were also characterized with peak-to-peak and root-mean-square values and with power spectral density analysis. The implications of these results are discussed in the context of operation beyond 100 kW, as well as the general viability of NHT technology for future mission applications.

*Ph.D. Candidate, Department of Aerospace Engineering, sjhall@umich.edu.
†Assistant Professor, Department of Aerospace Engineering, bjorns@umich.edu.
‡Robert J. Vlassic Dean of Engineering, Richard F. and Eleanor A. Towner Professor, and Arthur F. Thurnau Professor, Department of Aerospace Engineering, and Laboratory Director, PEPL, alec.gallimore@umich.edu.
§Senior Research Engineer, Electric Propulsion Systems Branch, hani.kamhawi-1@nasa.gov
¶Research Engineer, Electric Propulsion Systems Branch, thomas.w.haag@nasa.gov
‖Research Engineer, Electric Propulsion Systems Branch, jonathan.a.mackey@nasa.gov
**Research Engineer, Electric Propulsion Systems Branch, james.gilland@nasa.gov.
††Senior Research Engineer, Electric Propulsion Systems Branch, peter.y.peterson@nasa.gov
‡‡Ph.D. Pre-Candidate, Department of Mechanical and Aerospace Engineering, matthew.j.baird@wmich.edu

Nomenclature

g	Earth's gravitational acceleration, 9.81 m/s^2
I	current
j	current density
$\dot{m}$	mass flow rate
p	pressure
P	power
T	thrust
T/P	thrust-to-power ratio
TCFF	total cathode flow fraction
V	voltage
η	efficiency
Subscripts	
a	anode
b	background
c	cathode
d	discharge
I	inner channel
inj	injector
$keep$	keeper
M	middle channel
mag	magnet
O	outer channel
$P2P$	peak to peak
ref	reference
RMS	root mean square
t	total

I. Introduction

The next generation of electric propulsion (EP) systems—those in excess of 300 kW—can enable missions ranging from station-keeping of large Earth satellites to crew transport to Mars. Work by the Air Force Research Laboratory has shown that multi-hundred-kW EP systems can reduce LEO-to-GEO orbit transfer times to be comparable to chemical propulsion systems while allowing for nearly double the payload capability.[1] Further studies have demonstrated the need for 300-kW EP systems for station-keeping of large Earth satellites[2] and for cargo tugs for crewed missions in Earth-Moon space[3] and to near-Earth asteroids.[4] Other work has shown that >600-kW EP systems can be used for cargo or crew transport to Mars and its moons.[5–7] These systems would reduce trip times and increase deliverable payload. For crewed missions to these bodies and others, high-power EP systems offer benefits in trip time and payload capability that can increase astronaut time on the surface and reduce the number of launches necessary for a given mission.

While the need for high-power EP is apparent, there are multiple ways in which these systems could be realized. For example, a 300-kW system could consist of one large 300-kW thruster or an array of ten smaller 30-kW thrusters. The question of which configuration is optimum is one of cost, mass, performance, and footprint. Recent modeling efforts by Hofer[8] performed a systematic analysis of this question, taking real Hall thruster information from laboratory and flight programs to study propulsion system mass and cost trends. A major conclusion of that work was that 50 to 100-kW EP devices are a building block for missions up to 1-MW of total propulsion power. This covers all but the most ambitious future missions and strongly suggests the need to focus development efforts on thrusters of this class.

Hall thrusters are an attractive EP technology to be scaled to 50 to 100-kW-class devices for these high-power missions. Modeling has suggested that specific impulses on the order of 1500-2000 seconds are optimal to reduce trip times for human crews.[4,5] Ion thrusters (the only other EP technology with deep space flight heritage) typically provide efficiencies under 45% for these specific impulses[9] but Hall thrusters are capable of total efficiencies in excess of 60% at similar conditions.[10] With these advantages

in mind, NASA Glenn Research Center (GRC) undertook an effort to develop high-power Hall thrusters starting in 1999. This culminated in a series of 20-50 kW class Hall thrusters that demonstrated for the first time the performance capability of this technology at these power levels. The 50-kW class NASA-457Mv1 thruster, the highest-power thruster produced from this effort, was operated on xenon and krypton propellants through a range of operating conditions, demonstrating on xenon propellant a maximum total power of 96 kW, maximum discharge current of 112 A, maximum total efficiency of 0.58, and specific impulses from 1550-3560 seconds.[11–13] This thruster demonstrated scaling techniques and physical insight for creating high-power Hall thrusters. Previous to this effort, magnetic-layer Hall thrusters were typically 1–5 kW devices. Leveraging insight from this work, NASA developed a higher-fidelity version of the thruster named the NASA-457Mv2, which demonstrated improved performance over the v1 thruster,[14] though it was not tested beyond 50 kW discharge power. Additionally, the NASA-300M 20-kW thruster and NASA-400M 50-kW thruster were developed using similar scaling techniques, applying design lessons learned to continually improve performance.[10,15] This culminated in a demonstrated peak total efficiency of 0.67 at 500 V, 20 kW with the NASA-300M on xenon propellant. A 150-kW single-channel Hall thruster was even designed using these techniques but never built.[16] This thruster, designated the NASA-1000M, would have been 1 meter in diameter, the largest Hall thruster ever built.

While the GRC program was highly successful and demonstrated a road map toward 150-kW Hall thruster systems, one of the major challenges identified in this program (and exemplified by the NASA-1000M thruster design) was the excessively large footprint of higher-power systems. This is due to the fact that thruster diameter increases with power using these scaling techniques. One technique to avoid this issue and scale Hall thrusters beyond 50-kW class devices while limiting diameter increase is to concentrically nest multiple discharge channels around a shared centrally-mounted cathode. This technique allows for improved packing density of the channels as compared to multiple single-channel thrusters[17,18] while still relying on the proven channel scaling techniques developed by GRC. Two 10-kW class nested Hall thrusters (NHTs) have been developed, one by Busek Co., Inc.[19] and another by the University of Michigan.[20] The University of Michigan thruster, known as the X2, demonstrated the feasibility of multiple nested magnetic lens topologies and operation of multiple discharge channels from a single shared cathode, and generally forged a path for continued NHT development. In 2009, the University of Michigan, in partnership with the Air Force Office of Scientific Research, NASA, and ElectroDynamic Applications, began development of a three-channel, 100-kW class NHT known as the X3.[21–23] This thruster capitalized not only on the success of the X2 NHT but on the aforementioned series of high-power single channel Hall thrusters developed by NASA in the early 2000s. The X3 was first fired in 2013, but due to facility limitations at the University of Michigan characterization of the thruster to date has been limited to 30 kW.[22,24,25]

Though NHTs have shown promise to date, there still exist questions about the performance and high-power capability of the technology. The X2, a non-optimized demonstration thruster, displayed anode efficiencies in excess of 60% during its characterization but was only throttled to 500 V discharge voltage. The 30-kW characterization of the X3 showed surprisingly low performance for the larger channels, including 23% anode efficiency on the outer channel operating alone.[25] Previously proposed explanations for this anomalously-low performance include magnetic field and cathode coupling issues. There also remain questions regarding the mechanisms through which channels couple to one another. Early work on both the X2 and X3 showed a certain amount of cross-talk but these studies did not perform thorough investigations of the behavior.[26] Thus, the need is apparent to continue the development of NHTs, starting with characterizing the X3 at current densities and powers closer to nominal conditions in a facility with the necessary pumping speed.

Despite these potential concerns, NASA considers NHTs a promising technology and is funding continued development through the Next Space Technologies for Exploration Partnerships (NextSTEP) program, which is investing in the technologies that will be necessary for future crewed missions to Mars.[27] In total, three electric propulsion concepts are being funded by NextSTEP: the Variable Specific Impulse Magnetoplasma Rocket (VASIMR); the electrodeless Lorentz-force thruster; and the XR-100 nested Hall thruster system. The overall goal of the these projects is to demonstrate 100 continuous hours of 100-kW operation of the system operating at a total system efficiency in excess of 60%. The XR-100 system is being developed by a team led by Aerojet Rocketdyne (AR) and including the University of Michigan, NASA GRC, and the NASA Jet Propulsion Laboratory (JPL).[28] The system consists of the X3 NHT, a JPL-developed high-current hollow cathode,[29] and a power processing unit and xenon flow controller being developed by AR. Additional contributions include plasma and thermal modeling by JPL and facility and test infrastructure

by NASA GRC.

The 100-hour test is scheduled for 2018 at NASA GRC. A significant amount of infrastructure buildup was necessary in GRC's Vacuum Facility 5 (VF5) to support this test, details of which are provided below. In an effort to reduce the risk associated with this new testing apparatus, as well as to throttle the X3 through its operating envelope above 30 kW, a team of researchers from NASA GRC and the University of Michigan performed a risk reduction test for the NextSTEP program. This test involved firing the X3 in VF5 at total powers from 5 kW to 102 kW and was intended to identify any potential issues with the thruster or test setup at GRC prior to the 100-hour test. In doing so, we were simultaneously able to address a number of the remaining concerns about NHTs.

In this paper we focus on the performance mapping of the X3 during this risk reduction test. In Section II, we discuss the test hardware buildup at GRC, including a new thruster mounting cart, high-power thrust stand, electrical infrastructure, and data acquisition system. We also describe the plasma diagnostics included in the far-field region of the X3's plume, detailed results of which will be published in the future. Section III presents the measured thrust as well as calculated efficiency and specific impulse values. These results are presented in the context of other high-power Hall thrusters to show how the X3's behavior and trends compare to the state of the art. Additionally, discharge current behavior is presented with both oscillation amplitudes and power spectral densities. The results are discussed in the context of interaction between channels during multi-channel operation, future X3 operation, and potential mission applications in Section IV.

II. Experimental Apparatus

A. The X3 NHT

The X3, shown in Figure 1 firing in this test campaign, is a three-channel 100-kW class NHT developed by the University of Michigan's Plasmadynamics and Electric Propulsion Laboratory in collaboration with the Air Force Office of Scientific Research, NASA, and ElectroDynamic Applications.[30] The X3 is designed to operate efficiently on both krypton and xenon propellants from 200–800 V discharge voltage and at total discharge currents up to 250 A. The total power throttling range of the X3 is 2–200 kW. The thruster is approximately 80 cm in diameter and weighs 230 kg. Each of the three discharge channels features an inner and outer electromagnet for a total of six, each of which is controlled separately.

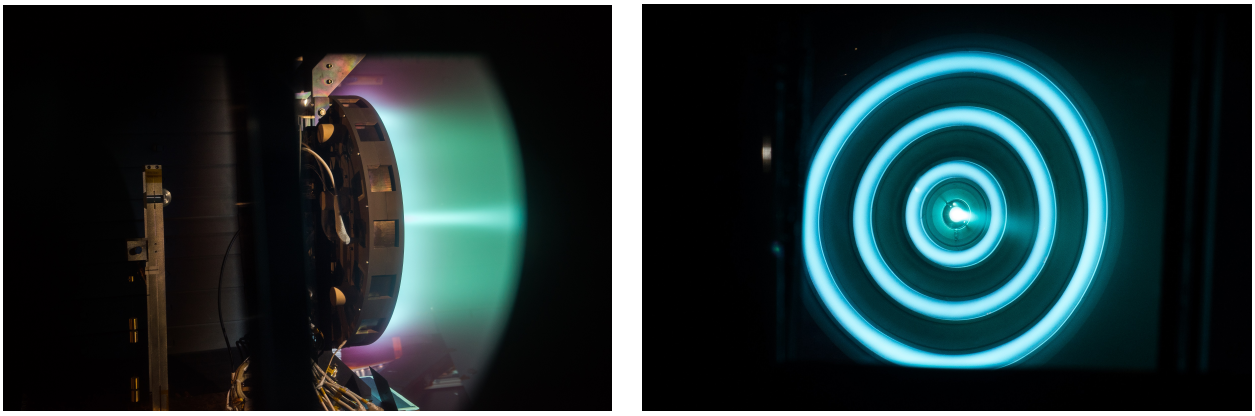

(a) Side

(b) End-on. Slight distortion is due to warping of the mirror used to take the photo.

Figure 1. Photographs from two angles of the X3 firing at 50 kW total discharge power in VF5 at NASA GRC.

Each of the X3's discharge channels can be fired separately or in combination with others, providing seven unique operating configurations. We denote these configurations throughout this paper using I for the innermost channel, M for the middle channel, and O for the outermost channel. For example, the configuration where the inner and middle channels are firing together is denoted as the IM configuration. The thruster operates off of a single high-current cathode capable of discharge currents in excess of 300 A. Both NASA JPL and NASA GRC have developed high-current cathodes for the X3.[29,31,32] The JPL

cathode (Figure 2) is being utilized for the NextSTEP program and was used for all testing described here. It features a lanthanum hexaboride (LaB_6) emitter and unique external gas injectors that reduce energetic ion production.[33] The total cathode flow fraction (TCFF) for this cathode is split between the cathode center and the injectors:

$$\text{TCFF} = \frac{\dot{m}_{c,t}}{\dot{m}_{a,t}} = \frac{\dot{m}_c + \dot{m}_{inj}}{\dot{m}_{a,I} + \dot{m}_{a,M} + \dot{m}_{a,O}}. \quad (1)$$

Work at JPL has identified 16 sccm as the optimized flow rate for the cathode center ($\dot{m}_c$), so any remaining flow of the TCFF is sent through the external injectors. For all but one test point here, the cathode was operated at a TCFF of 7% of the total anode flow (one test point was at 5%).

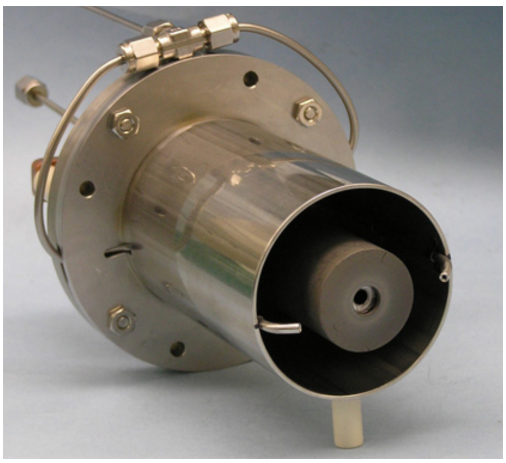

Figure 2. The JPL-designed high-current LaB_6 hollow cathode used during this campaign. The tubes at the 3 and 9 o'clock positions near the exit orifice of the cathode are the external gas injectors.

During this test campaign, the X3 was electrically isolated from the thrust stand inside the vacuum facility but then tied to facility ground on the atmosphere side of the test setup with a dedicated body grounding strap. The current collected by the grounded body was then recorded during testing. This current did not exceed 1.25 A, even during 250-A operation. This result is not unexpected, as the entire external surface of the X3, including the downstream faces of the pole pieces and the sides of the body, are treated with a dielectric coating. However, this is a significant result when comparisons are made to the grounded body current reported in other thrusters, which for instance is typically on the order of 10% of the discharge current for the NASA HERMeS Hall thruster.[34] The electrical configuration of a Hall thruster is an important testing concern but was beyond the scope of this test. The X3 has been grounded in all previous operation but was always grounded through the thrust stand such that collected current was not measured.

B. Vacuum Facility and Test Equipment

The testing described here was performed in Vacuum Facility 5 (VF5) at NASA GRC. VF5 is a 4.6 m diameter, 18.3 m long cylindrical vacuum chamber that features 33 m^2 of cryogenic pump surfaces, providing a pumping speed of 700,000 L/s on xenon. The facility walls and cryogenic panels are lined with graphite plates to minimize backsputter during thruster operation. Pressure inside the facility was monitored using four MKS Stabil Ion Gauges mounted in various locations. The pressures reported here are from the gauge mounted in the exit plane of the thruster approximately 1.5 meters from thruster centerline, pointed downstream. This gauge was calibrated on xenon and was corrected for orientation using techniques by Yim.[35] Facility base pressures were typically on the order of $1x10^{-7}$ Torr during this test campaign. Orientation-corrected background pressures while firing the thruster ranged from 4.3×10^{-6} to 4.2×10^{-5} Torr.

A new thruster support cart was designed specifically for the NextSTEP program. The cart rolls into VF5 through the endcap along the rail system inside the chamber and sits in front of the existing thruster testing location typically used for smaller thrusters such as the HERMeS thruster.[34,36,37] A schematic of the location of the X3 inside VF5, as well as the location of the plasma diagnostics package, is shown in Figure

3, and a photograph of the X3 NHT installed in VF-5 is shown in Figure 4. We operated the thruster off

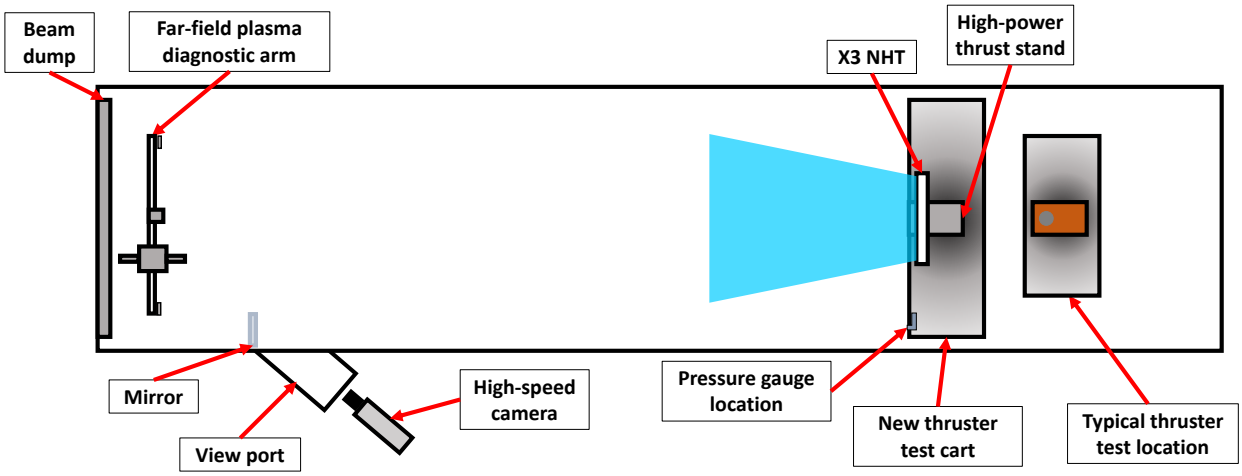

Figure 3. A schematic showing the location of the X3 as well as diagnostic equipment inside VF5. Schematic is not to scale.

of a set of laboratory power supplies, which included six separate supplies for the electromagnets, a cathode heater supply, and a cathode keeper supply. Each of the three channels was operated from a separate high-voltage, high-current power supply. The inner was operated using a set of three 1000 V, 15 A supplies that were connected in a master/slave configuration, the middle was operated using a 2000 V, 100 A supply, and the outer channel was operated using a 1000 V, 150 A supply. Additionally, during a small subset of operation outside of performance mapping all three anodes were operated with the 150-A power supply. Each discharge channel featured a 100 μF capacitor across the anode and cathode lines. These capacitors isolated the power supplies from the thruster and allowed the thruster to experience high-current transients without extinguishing. Electric propulsion-grade xenon propellant was provided to the thruster via five electropolished stainless steel feed lines. Each line featured a precision flow controller to prescribe the xenon: a 500-sccm controller for the inner channel, a 1000-sccm controller for the middle channel, a 2000-sccm controller for the outer channel, a 200-sccm controller for the cathode, and a 200-sccm controller for the cathode external injectors.

We measured thruster telemetry in a new breakout box developed at GRC for the NextSTEP program that leverages recent work done as a part of the HERMeS Hall thruster development. This breakout box contained precision shunts, voltage dividers, and isolation amplifiers that allowed for measurement of discharge, magnet, and cathode telemetry. This telemetry was collected by a data logger controlled by LabView. Telemetry was recorded at a rate of approximately 0.3 Hz. In addition to the low-speed measurements taken in the breakout box, high-speed measurements of the discharge currents were taken using a set of commercially-available current guns read by two commercially-available oscilloscopes. The discharge current oscillations were characterized using peak to peak (P2P) and root mean square (RMS) values that were calculated by the oscilloscopes and read by the telemetry data logger. Additionally, synchronized with acquisition of high-speed video as described below, we collected high-speed measurements of the discharge current of each channel, which were used for power spectral density analysis of the dominant oscillation frequencies.

C. Thrust Stand

We designed and built a new inverted-pendulum thrust stand capable of measuring up to 8 N of thrust for this test campaign. The stand was based heavily on the X3-dedicated thrust stand developed at UM previously.[38] The thrust stand operates in null mode, is calibrated in situ using a string of known masses, has active inclination control, and is water-cooled to protect against thermal drift during thruster operation, following industry best practices.[39–41] The thrust stand is approximately the same form factor as typical GRC-style thrust stands but features design modifications for the X3. To safely support the large mass of the X3, torsional bearing flexures are used in place of traditional thin-beam flexures. It features an optical displacement sensor in place of a traditional linear variable differential transducer, which improves sensitivity

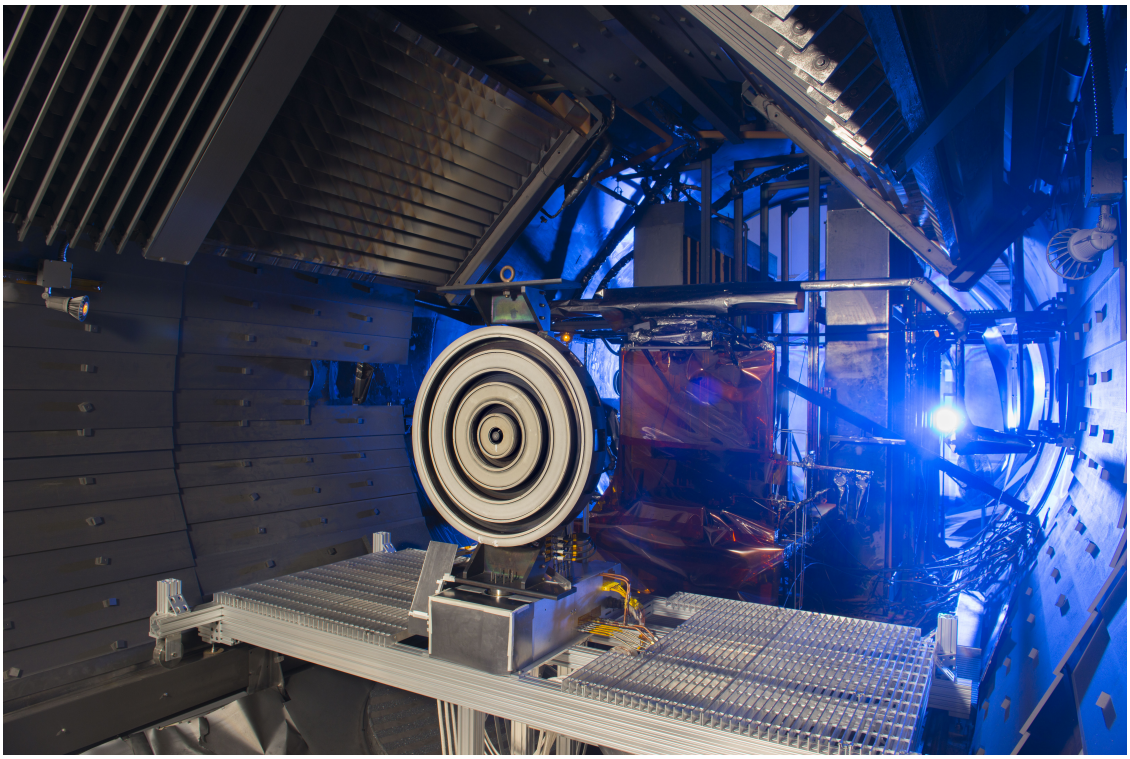

Figure 4. The X3 NHT installed inside VF5 at NASA GRC.

and reduces electrical noise by passing the signal through optical fiber in and out of the vacuum facility. The stand also features additional stainless steel propellant lines to accommodate the X3's requirements. We developed a new cable "waterfall" to pass discharge, magnet, and cathode power to the thruster, as well as thermocouple signals from the thruster. The waterfall was designed to minimize hysteresis on thrust measurement due to cable expansion and contraction by routing the cables perpendicular to the thrust axis. The X3's high discharge currents necessitate large-gauge wires and increase the importance of a properly designed waterfall.

Based on data collected throughout the test, the thrust stand was found to have a statistical uncertainty of approximately 2%, plus an additional 14 mN uncertainty due to the resolution of the inclination reading. We performed in situ calibrations of the stand at the beginning and end of each test day, and additionally took zeros periodically throughout the day. Over the course of this test campaign, we found that the thrust stand calibration slope (in mN/V) varied around the mean with a standard deviation of about 2% day to day. Thermal drift of the stand was typically around 1-2% of full scale across a day of operation. In an effort to assess whether electrical noise from thruster operation was affecting thrust measurements, a calibration weight was dropped during operation of the thruster in a particularly oscillatory condition. The thrust value for the weight matched the "thruster off" calibration value to within the thrust measurement uncertainty.

D. Other Diagnostics

We used a stationary far-field plasma diagnostics package to evaluate plasma plume properties of the X3. The plasma diagnostics package used here was provided by UM but relied on GRC diagnostic infrastructure and was operated similar to previous GRC plasma diagnostic work.[42,43] The package was positioned approximately 9 meters from the exit plane of the thruster near the beam dump of VF5. In an effort to limit setup complexity and possible failure modes, the diagnostics package was fixed to the chamber floor instead of mounted to motion stages. Figure 5 shows a photograph of the plasma diagnostic arm detailing the location of the various probes. These diagnostics included a retarding potential analyzer (to measure the average ion energy per charge for beam ions), a planar Langmuir probe (chiefly to measure plasma potential for correcting the retarding potential analyzer measurements, but also to measure floating potential and

electron temperature), a Wien Filter Spectrometer (to characterize the beam current and species fractions), and a set of four fixed Faraday probes (to characterize beam symmetry). Detailed diagnostics results will be presented in a future paper.

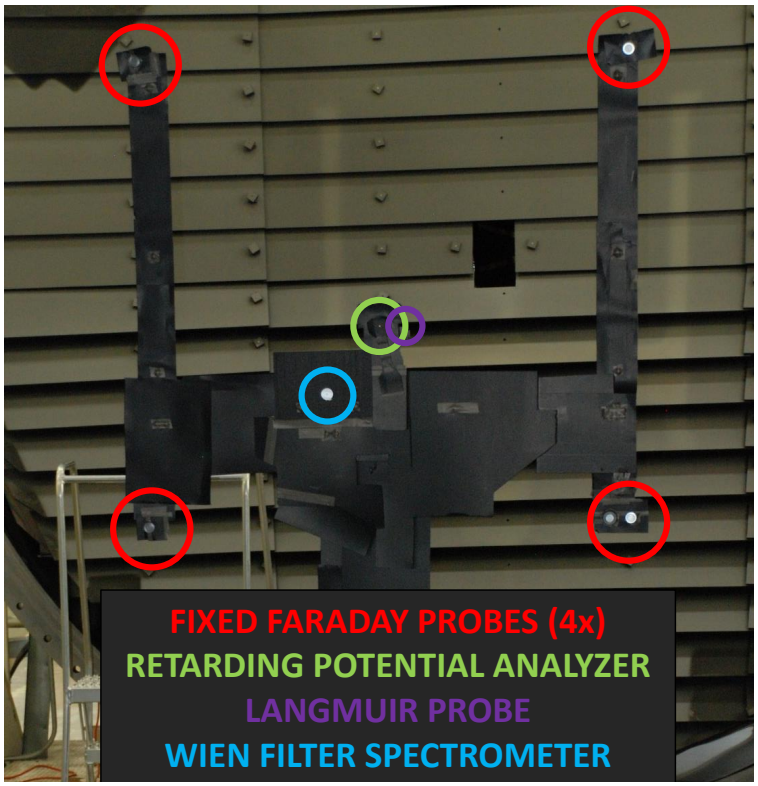

Figure 5. A photograph of the far-field plasma diagnostics arm used in this campaign with annotations denoting the location of each probe.

In addition to the high-speed discharge current traces captured via oscilloscope, high-speed video of the thruster was captured using a Photron SA-Z camera set up outside of the vacuum facility pointed at a mirror aimed at the X3. This setup is shown in Figure 3. These videos will be used to characterize the nature of the oscillation modes of each channel as well as the coupling between channels firing simultaneously. These results will be presented in a future paper.

III. Results

We successfully operated the X3 across a throttling envelope spanning 300–500 V discharge voltage and three current densities. Using the middle value as reference, these current densities were 0.63, 1.00, and 1.26 the reference value. All seven possible thruster configurations (I, M, O, IM, IO, MO, and IMO) were fired at each discharge voltage for the $0.63 \cdot j_{ref}$ and $1.00 \cdot j_{ref}$ conditions. For all test points, all firing channels were held at the same discharge voltage and current density. Additional test points were collected at 300 V and 400 V at the $1.26 \cdot j_{ref}$ condition, bringing the total unique test conditions to 46 for this performance characterization. We designed the test matrix to study the performance trends with both discharge voltage and current density, as well as to study how the performance varies for different channel combinations at fixed values of these parameters.

A. Thruster Operation

For all performance calculations here, the thruster was allowed to settle until the mean discharge current of each channel was stable and drifting no more than 0.01 A/min. We did not allow the thruster to come into thermal steady state during these measurements due to the length of time necessary to thermally soak the

thruster (expected to be in excess of 6 hours depending on the operating point). This concession is one made previously with large high-power Hall thrusters.[12] Although we did not operate the thruster in thermal steady-state, hours-long continuous operation at 50 and 80 kW indicated thruster performance and behavior was not changing significantly during thermal soaking. However, each channel of the X3 was thoroughly baked out at a given power level prior to any performance measurements at that power level. This incremental bakeout process was used to limit the risk from high-power operation. At each new discharge voltage/current density condition, the thruster would experience an initial period of discharge current instability, typically associated with moisture and other contaminants outgassing from the channel walls and other thruster components. Each channel was fired individually until this behavior passed (typically on the order of an hour at a new condition, but three to four hours the first time the thruster was fired after being exposed to atmosphere), and then we conducted performance characterization.

At each condition, we performed limited magnetic field mapping before collecting the performance data. We varied the magnetic field strength while maintaining the field shape, as is typical for Hall thrusters. The anode flow rate was held constant as well and was then adjusted as needed after the sweep was complete. During a sweep, thruster discharge, oscillation, and performance parameters were monitored. The optimal field strength for a given condition was that which provided the minimum discharge current. Typical sweep ranges were from 0.8 to 1.3 the reference field strength. Previous unreported X3 field sweeps were more extensive, and because the sweeps during this campaign matched the trends of those previous results we did not extend our range here. The reference field strength was the same for each channel and did not vary between single- and multi-channel conditions, although the magnet coil current ratios had to be modified in multi-channel operation, as explained in a companion paper.[44] Optimized field strengths across all conditions did not vary by more than 30%.

Due to the complexities involved in multi-channel magnetic field optimization (where the field of each channel affects the others), only minimal efforts were undertaken for multi-channel conditions. Typically, multi-channel conditions were simply operated at or near the optimum magnetic field strength found for single-channel operation at the given discharge voltage and current density. The field strength was kept constant for all firing channels for multi-channel operation. Because of this, we speculate that further performance optimization through magnetic field tuning may be possible for the multi-channel conditions, as will be discussed below.

B. Thruster Performance

Thruster performance is evaluated here using both anode and total quantities. The anode values provide an opportunity to compare thruster behavior while removing the electromagnets and cathode, neither of which has been optimized for flight, and the total values provide insight into how the X3 thruster will fit into the XR-100 system.

Anode efficiency is calculated as

$$\eta_a = \frac{T^2}{2\dot{m}_{a,t} P_{d,t}}, \tag{2}$$

where T is the measured thrust, $\dot{m}_{a,t}$ is total anode mass flow rate, and $P_{d,t}$ is total discharge power. Both $\dot{m}_{a,t}$ and $P_{d,t}$ are summed across all firing channels. Anode specific impulse is calculated as

$$I_{sp,a} = \frac{T}{\dot{m}_{a,t} g}, \tag{3}$$

where g is Earth's gravitational acceleration, 9.81 m/s^2.

Total values of efficiency and specific impulse are calculated very similarly to anode quantities, except that they include extra terms for the cathode and electromagnets. Total thruster efficiency is calculated as

$$\eta_t = \frac{T^2}{2\dot{m}_t P_t}, \tag{4}$$

where $\dot{m}_t$ is total mass flow rate:

$$\dot{m}_t = \dot{m}_{a,t} + \dot{m}_{c,t} \tag{5}$$

and P_t is total power:

$$P_t = P_{d,t} + P_{mag} + P_{keep}. \tag{6}$$

In Equation 5, $\dot{m}_{c,t}$ is total cathode mass flow rate (as described in Equation 1), and in Equation 6, P_{mag} is power to the electromagnets and P_{keep} is power to the keeper. Total thruster specific impulse is then calculated as:

$$I_{sp,t} = \frac{T}{\dot{m}_t g}. \tag{7}$$

Thruster telemetry values used in these calculations were averaged over a 60-second period.

The uncertainty in the thrust measurement was the dominant contribution to the uncertainty in efficiency and specific impulse calculations. Because the thrust uncertainty increased at lower thrust values (due to the constant-value uncertainty from the inclination resolution), lower-power conditions typically had slightly larger uncertainties in efficiency and specific impulse as well. Average uncertainties for specific impulse were $\pm$ 40 s and for efficiency were $\pm$ 0.04. Inner channel conditions typically were closer to $\pm$ 100 s and $\pm$ 0.06 because of their higher relative thrust uncertainty. These uncertainties are reflected in the error bars on the plots below.

Figure 6 presents thrust as a function of discharge power. For the conditions tested, the X3 produced a maximum thrust of 5.42 N ($\pm$ 0.1 N) at 98.4 kW discharge power (400 V, 247 A). At 101 kW discharge power (500 V, 201 A) the X3 produced 5.03 N ($\pm$ 0.1 N). At a fixed discharge voltage, the X3 operated at a similar thrust to power ratio (T/P) in each of the seven channel combinations. Average T/P values are plotted alongside the data in the figure and are compared to those of other NASA high-power Hall thrusters in Table 1. As shown in the table, the average T/P results are slightly improved over those of other high-power Hall thrusters, indicating that the X3 is operating as designed. These results also demonstrate that the T/P value attained is not dependent on the channel combination. This was not the result seen during previous low-power, low-current density operation of the X3 at PEPL.[25] We present a discussion of potential reasons for this improved performance in Section IV.

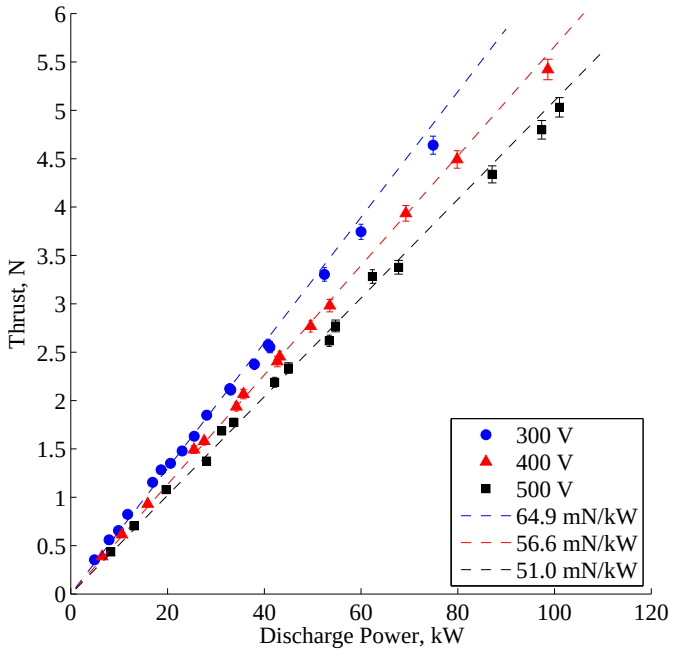

Figure 6. X3 thrust versus total discharge power. Error bars are plotted for all test points; for all but the highest-thrust measurements, these error bars are within the size of the marker. Lines of average thrust to power ratio for each discharge voltage are also plotted.

Table 1. The average thrust-to-power values for the X3 and other NASA high-power Hall thrusters for each discharge voltage tested.

V_d	NASA-457Mv1	NASA-400M	NASA-300M	X3 NHT
300 V	57.8 mN/kW	59.0 mN/kW	63 mN/kW	64.9 mN/kW
400 V	51.9 mN/kW	49.7 mN/kW	56 mN/kW	56.6 mN/kW
500 V	47.2 mN/kW	47.4 mN/kW	50 mN/kW	51.0 mN/kW

Figure 7 shows anode and total specific impulse as a function of discharge power. We found that the anode specific impulse for the conditions tested ranged from 1930–2150 seconds (± 50 seconds) for 300 V, 2190–2470 seconds (± 50 seconds) for 400 V, and 2480–2840 seconds (± 60 seconds) for 500 V, and that except for a low-power drop off, specific impulse for a given discharge voltage were roughly constant. This trend was true regardless of channel combination. Because of the large number of channel combinations for the X3, these different configurations are not noted in these figures for clarity. The X3's values match those found for other high-power Hall thrusters, as shown in the anode specific impulse ranges presented in Table 2. The NASA-300M showed specific impulse values that increased with power for a given discharge voltage (c.f. Figures 6 and 7 by Kamhawi[10]), a trend similar to that demonstrated by the X3 here.

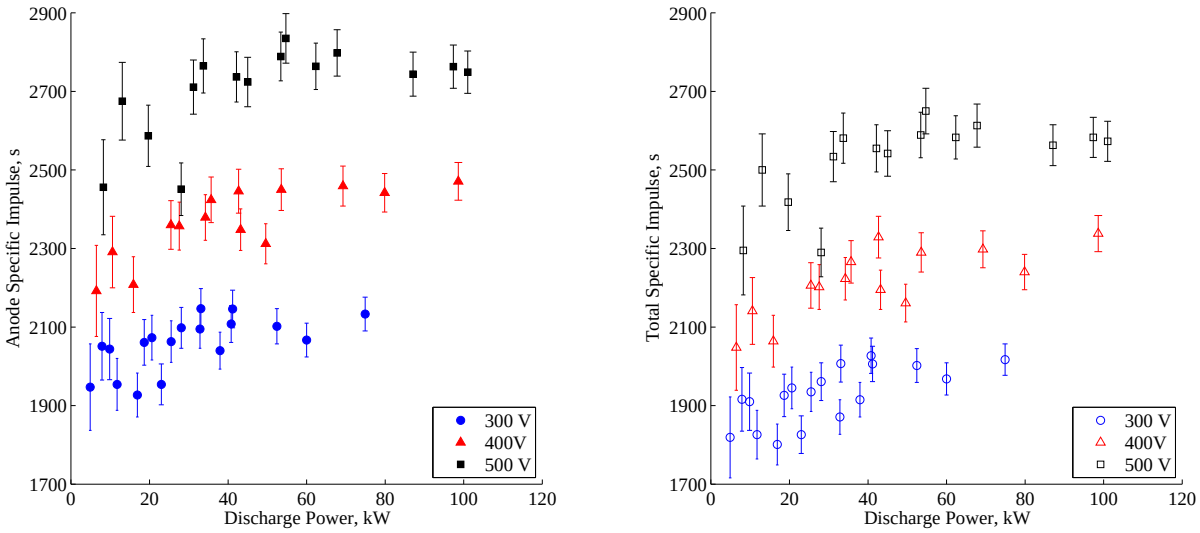

(a) Anode specific impulse

(b) Total specific impulse

Figure 7. X3 specific impulse as a function of discharge power for different discharge voltages. Error bars indicate the statistical uncertainty in the measurement for each point.

Table 2. Comparison of anode specific impulse ranges at different discharge voltages from the X3 and other NASA high-power Hall thrusters.

V_d	NASA-457Mv1	NASA-400M	NASA-300M	X3 NHT
300 V	1750–2100 s	1700–2100 s	1900–2200 s	1930–2150 s
400 V	2100–2400 s	2000–2600 s	2200–2600 s	2190–2470 s
500 V	2400–2750 s	2500–3000 s	2500–2900 s	2480–2840 s

Table 3 presents the anode efficiency ranges and averages for the X3 versus discharge voltage, as well as ranges for other high-power Hall thrusters. Anode efficiency is used for this comparison because total efficiency values were not published for all other thrusters. It can be seen that the average efficiency of the X3 trends upwards with increasing discharge voltage, a trend shared with the other thrusters. In addition,

the efficiency at a given discharge voltage increases from the NASA-457Mv1 to the NASA-400M to the NASA-300M. This is due to the fact that each subsequent thruster benefited from lessons learned from those before it. For example, the NASA-400M implemented an improved magnetic field design based on lessons learned in the NASA-457Mv1 and NASA-173M development that was intended to improve the efficiency of its operation.[45,46]

Table 3. Comparison of anode efficiency ranges at different discharge voltages from the X3 and other NASA high-power Hall thrusters.

V_d	NASA-457Mv1	NASA-400M	NASA-300M	X3 NHT range	X3 NHT avg.
300 V	0.50–0.57	0.55–0.59	0.60–0.67	0.62–0.71	0.66
400 V	0.53–0.60	0.60–0.65	0.55–0.73	0.63–0.71	0.66
500 V	0.46–0.65	0.66–0.71	0.60–0.73	0.58–0.72	0.68

During this test, the X3 operated at a peak total efficiency of 0.64 ($\pm$ 0.03) at 400 V and 0.67 ($\pm$ 0.03) at 500 V. In general, the total efficiency was approximately 0.05 lower than anode efficiency regardless of operating configuration, as can be seen in the throttle tables presented in the Appendix. For reference, the NASA-300M demonstrated peak total efficiencies of 0.67 at 400 V and 0.66 at 500 V. Thus, it is apparent that the X3 is operating at the state of the art, and continued magnetic field optimization may even further increase these values.

C. Comparison of Single-channel and Multi-channel Operation

1. Performance

With three discharge channels operating in close proximity, there is the expectation that coupling between the channels could effect performance. Indeed, previous experiments with the X2 10-kW two-channel thruster demonstrated that that device produces increased thrust of up to 11% when firing both channels simultaneously as compared to the sum of each channel firing individually. A recent test campaign by Georgin[47] and Cusson[48] investigated this phenomenon in more detail and found that the thrust increase was replicated when flowing propellant through the non-firing channel in single-channel mode. They attributed this effect, and the changes observed in the plasma that they found to be causing the increase in thrust, to be due to the change in the pressure field close to the thruster caused by the flow from the adjacent channel. Beal identified similar trends in a cluster of 200-W Hall thrusters, finding that a single thruster could couple normally with a cathode on the other side of the two-thruster cluster if propellant was flowing through the intermediate thruster.[49] Plasma plume measurements suggested that this extra neutral flow was likely improving electron transport across field lines via collisional effects. Unfortunately, thrust was not measured in that study, so it is unclear whether there was a performance effect due to the increased local neutral pressure.

We operated the X3 in its single- and three-channel configurations for seven different combinations of discharge voltage and current density. Figure 8 presents the thrust produced by the X3 at each of its IMO-configuration points alongside the summed thrust from the I, M, and O configurations at the same conditions. Error bars reflect the thrust measurement uncertainty for each point, typically around 2%. We found that the summed I, M, and O conditions typically produced slightly more thrust than the IMO condition, but that in general the measurements matched to within their uncertainty.

2. Oscillatory Behavior

Discharge current oscillations have been shown to affect Hall thruster performance[50] and their effects have been proposed to have roles in thruster processes such as anomalous transport[51,52] and cathode erosion.[53] Work has shown that the magnetic field strength is a strong driver of oscillation strength and character in unshielded Hall thrusters.[50] Characterizing discharge current oscillations was an important part of understanding operation of the X3.

We collected peak-to-peak (P2P) and root-mean-square (RMS) measurements of the discharge current oscillations during this performance mapping campaign. These measurements were made by the current guns and oscilloscopes described above in Section II and read by the data logger during telemetry measurement cycles. The values presented here are averaged over the same 60 second period as the telemetry used in the performance calculations. For simplicity, only the P2P values are presented. The RMS values showed

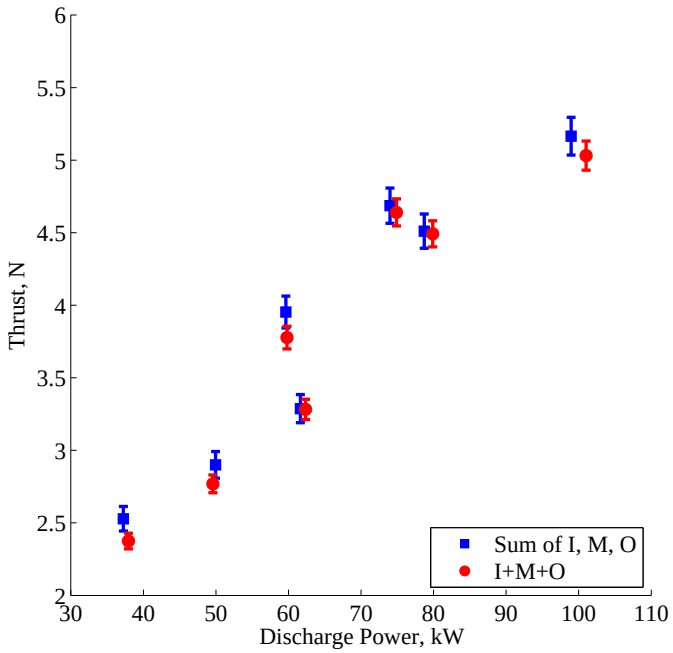

Figure 8. Comparison of three-channel thrust and comparable summed single-channel thrusts for the X3.

similar trends between conditions but in all cases were a smaller percentage of the mean discharge current. Figure 9a presents the P2P values normalized by their respective channel's mean discharge current. Single- and multi-channel conditions are indicated by closed and open markers, respectively. Figures 9b–d show the average values for each channel in single- and multi-channel operation for each discharge voltage tested. The error bars on the bar charts represent the standard deviation of the values for each case.

The figures show that P2P values for all three channels were less than 40% for single-channel operation at all discharge voltages. The outer channel's oscillation strength typically was unchanged or grew slightly in multi-channel operation but remained below 50% for all but a single condition (at 500 V). The middle channel's oscillation strength grew slightly more in multi-channel operation, rising to an average of about 50% for 300 V and 400 V and closer to 75% for 500 V. The inner channel experienced the largest difference in oscillation strength between single-channel and multi-channel operation, rising from a single-channel average less than 40% the mean values (comparable to the other two channels) to a multi-channel average approximately 70% at 300 V and 400 V and an average approaching 100% at 500 V.

Additionally, at each performance test point we collected high-speed discharge current measurements using the current guns and oscilloscopes described above. We applied a fast Fourier transform to these results, and from that calculated a power spectral density (PSD). These PSDs provide insight into the dominant oscillation frequencies and their relative strength. With multi-channel operation, they also provide insight into whether channels are synchronizing frequencies or experiencing cross-talk (where the peak of one channel's PSD appears in that of another). Figure 10 presents an example set of discharge current PSDs. For each channel combination at 400 V and $1.0 \cdot j_{ref}$, we calculated PSDs for each firing channel. We smoothed these results using a Savitzky-Golay filter for clarity in the figures.

A relatively broad peak around 10 kHz can be seen in all of the traces, which is identified as the breathing mode, a mode that is typically on the order of 1-20 kHz in Hall thrusters.[54] The similarity in quality of these peaks indicates that the thruster is generally operating in a similar oscillation mode across the configurations. In multi-channel modes, the breathing frequencies often appear to be synchronized (e.g., IO and MO), though one notable exception is the IMO condition where the inner channel is clearly breathing at a lower frequency than the middle and outer channels. In addition to this breathing frequency, a higher-frequency (60–80 kHz) peak is detectable in some of the X3 traces. This higher-frequency peak does not show synchronization in

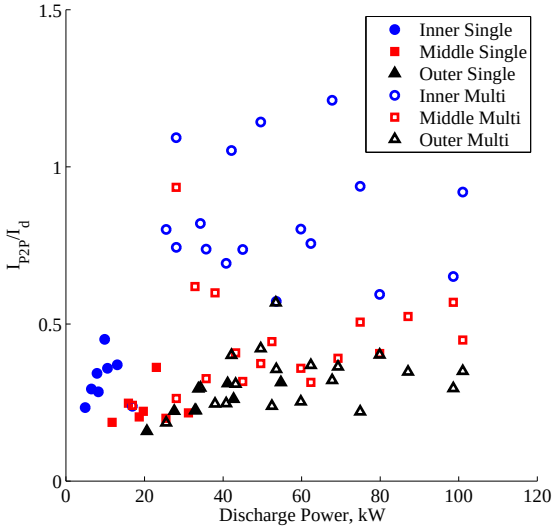

(a) P2P versus discharge power for all test conditions.

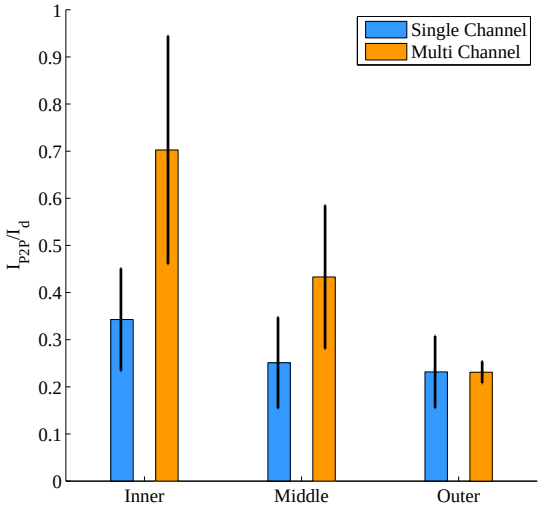

(b) 300 V average P2P values for each channel in single- and multi-channel operation.

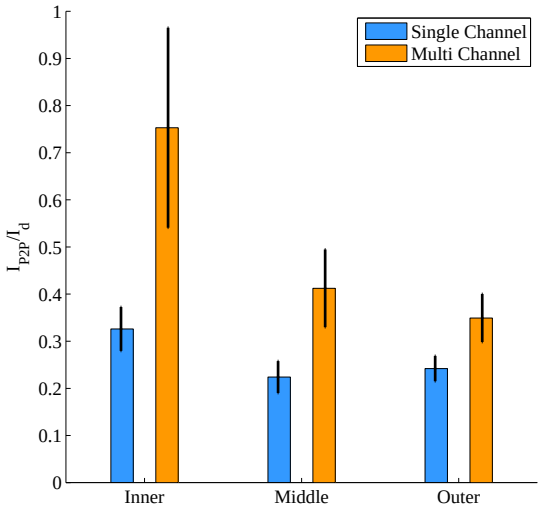

(c) 400 V average P2P values for each channel in single- and multi-channel operation.

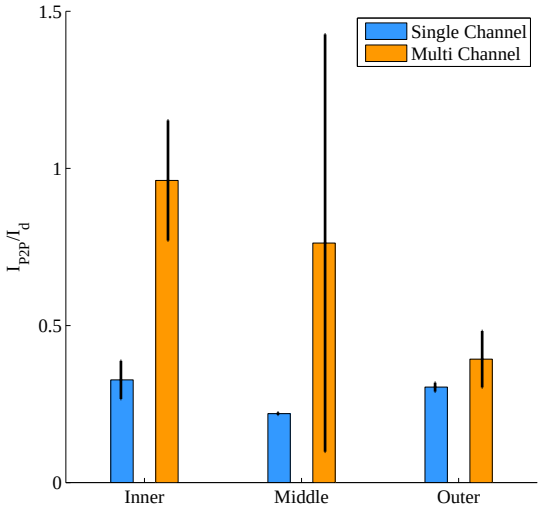

(d) 500 V average P2P values for each channel in single- and multi-channel operation.

Figure 9. Peak-to-peak discharge current oscillation values normalized by the mean discharge current for that channel. Error bars on bar charts represent standard deviation of data.

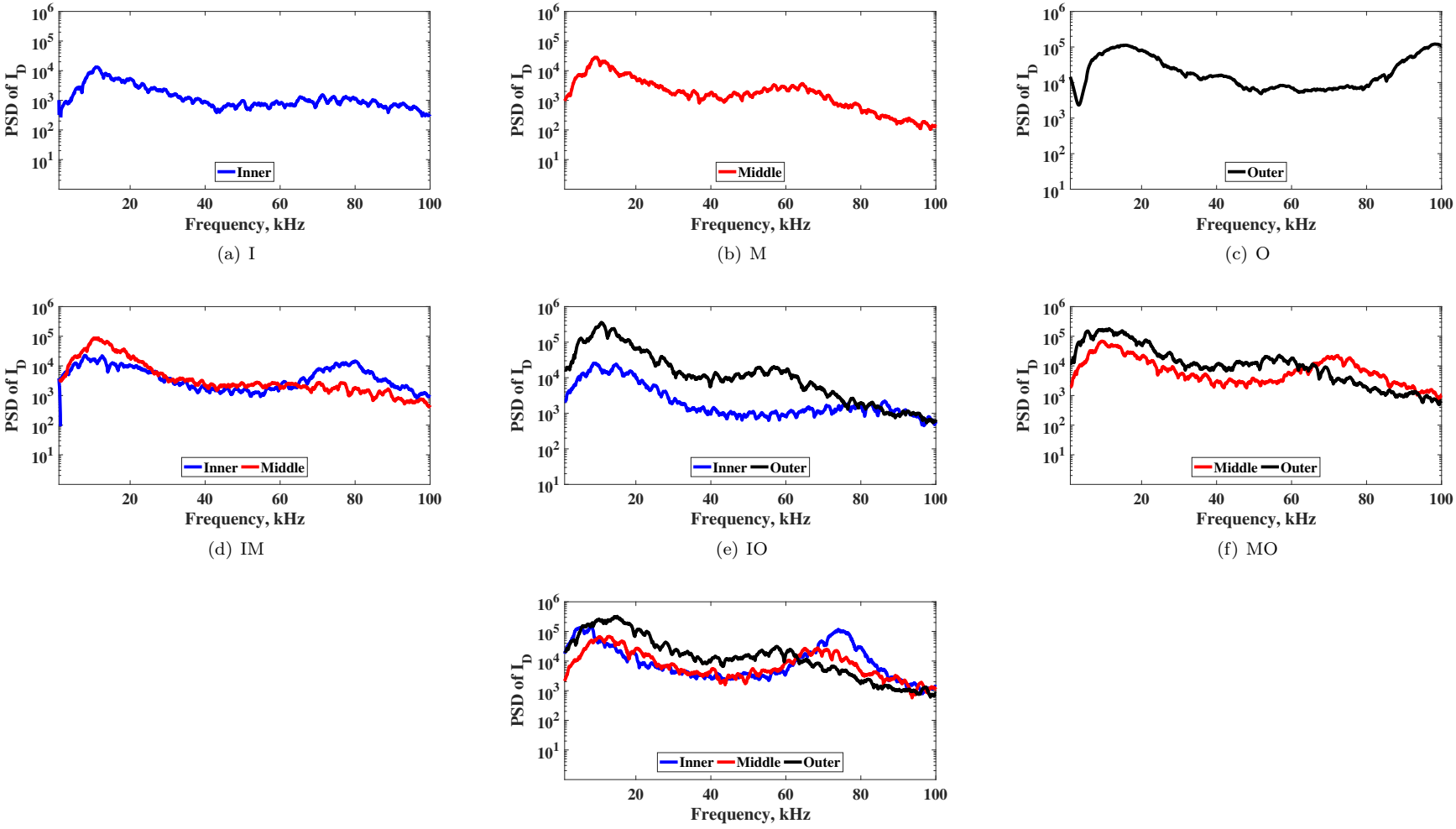

(a) I (b) M (c) O

(d) IM (e) IO (f) MO

(g) IMO

Figure 10. Discharge current PSDs for each channel combination for the X3. These results are from the 400 V, 1.0·j_{ref} condition.

multi-channel operation. In fact, this peak generally stays constant for a given channel, and its frequency decreases for larger channels: the inner's peak is typically around 80 kHz, the middle's 70 kHz, and the outer's 60 kHz.

3. Cathode Coupling

Another metric to compare the operation of the X3 in single-channel and multi-channel modes is the cathode-to-ground voltage (V_{cg}). Hall thruster cathode-to-ground voltage is typically between 5 and 30 V below facility ground, and is a metric of how well the thruster is coupling to the cathode.[55–57] Values of V_{cg} that are smaller (less negative) are indicative of improved coupling, and these smaller values allow for more of the thruster discharge voltage to be available for ion beam acceleration. Substantial differences in V_{cg} between single- and multi-channel conditions for the X3 would indicate that the thruster is coupling to the cathode differently between these conditions. Figure 11 presents V_{cg} for both single- and multi-channel X3 operation as a function of discharge power. The TCFF was held at 7% of the anode flow for all test points here except one; this test point, at 5%, featured a V_{cg} of –10.9 V, no different than the rest of the conditions. The data show that V_{cg} varied between –8 and –14 V across all conditions and power levels tested here, showing no significant difference between single- and multi-channel operation and demonstrating no trend with discharge power.

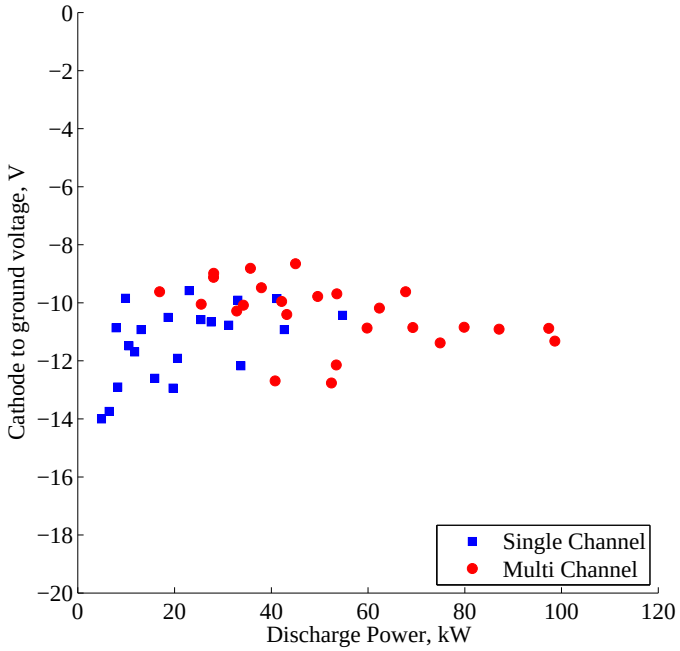

Figure 11. Cathode-to-ground voltage versus discharge power for all test conditions. Single- and multi-channel conditions are noted by square and circle markers, respectively.

IV. Discussion

A. Performance

The X3 was designed to leverage the physical insight and lessons learned from previous NASA single-channel high-power Hall thruster development. The results presented here indicate that this effort was successful. The X3 demonstrated T/P, efficiency, and specific impulse values that are comparable or in excess of that family of high-power Hall thrusters, and that showed similar trends with discharge voltage and power. The thrust was approximately linear for a given discharge voltage, and average T/P values matched those of the

NASA-300M. Specific impulse was generally constant for a given discharge voltage, except at low powers. This trend is likely attributable to the fact that Hall thruster performance decreases at low current densities. The lower-specific impulse conditions for the X3 were at the lowest current density, 0.63 $\cdot j_{ref}$. The NASA-300M showed similar trends in specific impulse with discharge power (for fixed discharge voltage). All of these results indicate that the NASA-style Hall thruster scaling as developed by NASA GRC is applicable to the NHT configuration with equal success as was achieved with single-channel Hall thrusters, regardless of channel combination. These results differ from those of the 30-kW performance characterization of the thruster,[25] which indicated that the middle and outer channels were under-performing expected values. We speculate that the improved performance here is a product of one or more factors. These include improved magnetic field settings as a result of a more thorough modeling effort,[44] a number of thruster modifications made as part of the preparation for this risk reduction test, and the improved background pressures in VF5.

In addition to the high performance across the throttle table, these results represent a number of new achievements for laboratory Hall thruster operation. To date, the NASA-457Mv1 thruster demonstrated the highest total power operation (96 kW), the highest discharge current operation (112 A), and the highest thrust recorded (3.3 N), all reported by Manzella.[11] Here we demonstrated the X3 at different conditions to 102 kW total discharge power and 247 A total discharge current, and recorded a maximum thrust of 5.42 N (at 99 kW, 400 V).

The X3's demonstrated performance and extended Hall thruster power, discharge current, and thrust operating envelopes have important implications for the application of Hall thrusters to forthcoming missions. As discussed in the introduction, the need is apparent for electric propulsion systems operating at power levels in excess of 300 kW and specific impulses of 1500–3000 seconds, and that modeling work suggests that these systems should consist of individual thrusters on the order of 50–100 kW to minimize both system cost and mass. Our results demonstrate for the first time NHT operation at 100 kW. Although the X3 has yet to be throttled up to its full design power of 200 kW, these results have further implications beyond simply demonstrating 100-kW operation. The NASA-457Mv1 100-kW operation was at 845 V discharge voltage, providing a total specific impulse of 3460 seconds, and demonstrated a total efficiency of 0.58. The 100-kW operation of the X3 here was at 400 V and 500 V discharge voltage and demonstrated total efficiency of 0.63 at both points. This lower-voltage operation provided total specific impulses of 2340 s at 400 V and 2570 s at 500 V, values squarely within the 1500-3000 second range identified by mission planners as ideal for cargo tugs and crew transport to destinations such as Mars.[5,7] With these results, the X3 has demonstrated that Hall thrusters—and more specifically NHTs—are a viable propulsion option for upcoming high-power space missions of many types.

Based on these results at moderate discharge voltages, we can project expected performance values for the X3 at higher discharge voltages based on the trends seen in other high-power Hall thrusters. We expect that the X3 will continue to operate comparably to these thrusters as the discharge voltage is increased to 800 V. Previous results indicate that the T/P ratio should continue to decrease with increasing V_d, and based on the X3's average T/P values here we expect an average T/P of 40 mN/kW at 800 V discharge voltage. This should produce thrust values of 4 N at the 100-kW condition and 8 N at the 200-kW condition. Specific impulse should continue to increase with increasing discharge voltage, resulting in total values of 3500–3600 seconds at 800 V discharge voltage. Efficiency typically increases with increasing discharge voltage for Hall thrusters with a magnetic lens field topology.[46] Based on the fact that the X3 followed the trends of other NASA high-power Hall thrusters in efficiency at the voltages tested here, we expect that the X3 may be capable of anode efficiencies approaching 0.75 at 800 V, equivalent to total efficiencies approaching 0.70.

B. Multi-channel Operation Effects

There remain open questions regarding how the channels of NHTs communicate with and affect one another while operating simultaneously. These data provide a certain amount of insight to these potential mechanisms. One possible manifestation of channel communication would be in the performance: adjacent channels firing simultaneously could perhaps cause an increase or decrease in thruster performance due to localized effects. However, these data suggest that this is not occurring significantly with the X3, and that for a given discharge voltage and current density, each channel combination produces comparable performance. This is in stark contrast to previous work with the X2 10-kW NHT, which showed a thrust boost of 5–11% in dual-channel mode, a boost that would be well outside of the uncertainty of the measurements here. There are a number of possible explanations for this behavior:

1. We operated the X3 here in a constant-discharge current manner, adjusting the mass flow to achieve the target discharge current. This was selected due to the range of background pressures experienced during typical X3 operation. By throttling to target discharge currents, any background ingestion experienced by the thruster is accounted for and more direct performance comparisons can be made. Georgin and Cusson ran the X2 in a constant-mass flow manner for their work and did not report on thruster ingestion or changes in discharge current due to this effect, so it is unclear what role this may have had on their results. Liang, however, found the 9% thrust boost in his tests for constant mass flow rate (and background pressure) accompanied negligibly-small discharge current changes due to ingestion, so we suspect that our controlling for this does not account fully for the X3's behavior.

2. For single-channel operation, we only powered the magnets for the channel that was firing. This is different than work with the X2, where all four magnets of the thruster were left on throughout the test. Because we tuned the field strength at each condition, it is possible that we have obscured a trend that would be present if we operated the X3 such that magnetic fields were kept constant throughout I, M, O, and IMO operation.

3. The X3's cathode features downstream neutral injectors, as discussed above. These injectors were flowing at least small amounts of xenon during all M and O operation and during some I operation. Both the X2 work and Beal's work with thruster clusters demonstrates that neutral flow plays a large role in the behavior of multiple Hall thruster discharges in close proximity. Additional work by Brown has shown that near-cathode neutral injection can stabilize Hall thruster discharges.[58] A possible explanation for the X3's lack of apparent thrust boost is that the cathode neutral injectors are acting in a similar fashion to the neutral propellant that both research teams flowed through their non-firing anodes. The enhanced neutral pressure in front of the X3 due to these injectors may be affecting the discharge in the same way, thus actually raising the single-channel performance to match that of the IMO condition, which experiences the multi-channel enhanced neutral pressure similar to the X2.

4. The X2's channels are scaled differently than those of the X3. It is possible that NASA-style HET scaling is less susceptible to these effects, or that another difference in design of the thrusters (unrelated to channel scaling) makes the X3 impervious to the effects observed on the X2.

Uncertainty of the measurements aside, it appears that the IMO condition produced less thrust than the sum of the I, M, and O conditions for certain cases, opposite the trend found with the X2. However, we expect that this is a product of magnetic field settings and not some kind of multi-channel loss mechanism at work. Because the single-channel conditions generally went through more rigorous magnetic field optimization than what was done for the IMO condition, it is not surprising that these conditions were producing slightly more thrust. We suspect that additional magnetic field tuning would bring the thrust of the IMO conditions up to match the sum of the single-channel thrusts. Further work, including more detailed magnetic field optimization, mapping the pressure field in front of the thruster with the injectors flowing, and operating the X3 in a similar manner as work with the X2, is necessary to fully explore this behavior.

Another mechanism of communication between channels is through the oscillations. As we show in Figure 9, the peak to peak oscillations vary between single- and multi-channel operation for the inner channel and to a lesser extent the middle channel, yet stay roughly constant for the outer. One potential explanation for this involves changes in magnetic field between single- and multi-channel operation. This effect is explored in a companion paper.[44] Compared to single-channel operation, the outer channel's electromagnets operate at nearly the same settings in multi-channel operation. However, the magnet current ratios for the inner and middle channels change significantly between these conditions due to the way that magnetic flux is shared among the magnetic circuit of the thruster. We found at times during multi-channel operation that the inner and middle channels had areas of deposited carbon on the discharge channel walls that were glowing orange, indicating that plasma was impinging on the walls in a location different than during single-channel operation when these bands were established. At times of intense burn-off, the discharge current oscillations grew very large. Though we made an effort to minimize or burn off these spots before taking performance measurements, this change in plasma location could still be contributing to the change in oscillation character through these wall effects. It is also possible that the different field ratios for the inner and middle channels during multi-channel operation resulted in a change in I-B characteristic,[50] and that a change in field strength on those channels would have reduced the oscillations. Additionally, some other type of channel coupling effect could be at work. For instance, though the channels were by no means experiencing the same P2P

values when operating together, it is possible that the larger P2P values for the outer channel were in some way being spread to the other channels, perhaps via the cathode. Typically, the cathode P2P values matched the maximum value from which ever channels were firing. For IMO operation, this was typically the outer channel. The way the other two channels experience oscillations while coupling to a cathode with P2P values in excess of 100% of their mean discharge current is unclear, but it is possible that these larger oscillations were, to a certain extent, making their way to the other channels. Further work is necessary to fully characterize these effects, including analysis of the high-speed camera data. Ultimately, though the inner channel's multi-channel oscillations were stronger than the rest, the X3's P2P oscillations did not fall outside of the range typically seen by Hall thrusters.[37]

As shown in the PSDs in Figure 10, the frequency and nature of the oscillations for a given channel do change somewhat between operating configurations. However, they do not change drastically for a given discharge voltage and current density, suggesting that these small changes may be due to small changes in the magnetic field settings between channels as opposed to any cross-talk effects. There are some features of the PSDs that are of interest, in particular the high-frequency peak that changes frequency and shape with channel but stays approximately constant regardless of whether channels are operated together. Previous work on oscillations by Choueiri has suggested oscillations of these frequencies (20–100 kHz) could be related to processes inside the discharge channel related to neutral collisional processes, ionization, or a combination of both.[54] Other work has suggested that these oscillations are cathode-related, such as work by Jorns with a 6-kW laboratory Hall thruster in both magnetically shielded and unshielded configurations.[59] They demonstrated peaks in similar locations in both the light intensity from a high-speed camera and in the discharge current PSDs. Their work suggested that these higher-frequency modes may be gradient-driven and cathode-related. They found that the higher-frequency cathode peak became less coherent as it propagated radially outward. This behavior may explain the decrease in frequency and the increase in width of this peak in successively larger channels of the X3. However, it is also possible that a cathode-based oscillation would be at the same frequency throughout the discharge, which would suggest that this oscillation is related to phenomena inside the channel. The high-speed camera data collected during this test will provide further insight into the nature of these oscillations.

One more potential mechanism through which the channels of an NHT may affect each other or differ in operation at a given condition is through coupling to the cathode. However, the X3 data suggest that cathode coupling was consistent across all conditions and power levels tested, indicating that cathode coupling is not a function of channel combination or power level. One possible explanation for this is related to the discussion of multi-channel performance above. The increased neutral flow near the cathode (via the external cathode injectors) may be responsible for enhancing cathode coupling in a manner similar to that described by Beal.[49] Because of the way the channels are scaled, the larger the channel, the more auxiliary flow needed during operation to provide the proper TCFF. This increasing neutral flow field in front of the thruster may be enhancing the cathode coupling for larger channels and overcoming potential negative effects such as distance between channel and cathode. Further work, including firing the larger channels without auxiliary flow, may help identify this mechanism.

V. Conclusions

We successfully measured the performance of the X3 for a range of conditions spanning total power levels from 5 to 102 kW. These conditions consisted of discharge voltages from 300 to 500 V and current densities that were 0.63, 1.00, and 1.26 of a reference value. The seven channel combinations of the thruster were throttled across this range of settings. For each test point, we directly measured thrust using a high-power inverted-pendulum thrust stand, and from those thrust measurements and thrust telemetry, we calculated specific impulse and efficiency values. We collected measurements of the discharge current oscillations at each point to assess thruster stability. Additionally, far-field plasma diagnostics and high-speed video measurements were collected, detailed results of which will be published in a future paper.

Our results demonstrated that a three-channel 100-kW class NHT can offer comparable or even improved performance over high-power single-channel thrusters. The X3 demonstrated total efficiencies ranging from 0.54–0.67 and total specific impulses from 1800–2650 seconds, experiencing the peak efficiency at 500 V discharge voltage. Additionally, the results indicate that none of the available channel combinations were significantly over- or under-performing the rest, demonstrating comparable specific impulse and efficiency at a fixed discharge voltage and current density. The sum of the single-channel thrusts generally was not

significantly different than the three channels operating together for a given discharge voltage and current density, a surprisingly result that differed from previous NHT testing. Ultimately, the X3 demonstrated new levels of Hall thruster power (102 kW), thrust (5.4 N), and discharge current (247 A). These results demonstrate the capability of Hall thrusters and NHTs for cargo and crew transport applications and show that the X3 represents a significant milestone on the roadmap to Mars.

Appendix

Table 4. 300 V throttle table for the X3 performance measurements.

$V_{d,I}$ V	$I_{d,I}$ A	$V_{d,M}$ V	$I_{d,M}$ A	$V_{d,O}$ V	$I_{d,O}$ A	$P_{d,t}$ kW	T N	$I_{sp,a}$ s	$I_{sp,t}$ s	η_a –	η_t –	V_{cg} V	p_b μTorr
300.2	16.3	0	0	0	0	4.9	0.35	1950	1820	0.69	0.64	-14.0	4.6
0	0	296.4	39.6	0	0	11.7	0.82	1950	1830	0.67	0.62	-11.7	10.2
0	0	0	0	300.3	68.6	20.6	1.35	2070	1950	0.67	0.62	-11.9	15.9
300.0	16.5	301.0	39.7	0	0	16.9	1.15	1930	1800	0.65	0.60	-9.6	13.8
300.0	16.0	0	0	300.4	68.9	25.5	1.63	2060	1940	0.65	0.60	-10.1	18.5
0	0	303.3	39.0	300.3	70.0	32.9	2.12	2100	1870	0.66	0.58	-10.3	23.0
299.8	16.5	303.1	39.4	300.3	70.1	37.9	2.38	2040	1920	0.63	0.58	-9.5	25.5
299.5	26.4	0	0	0	0	7.9	0.56	2050	1920	0.71	0.66	-10.9	6.6
0	0	292.6	63.8	0	0	18.7	1.28	2060	1930	0.70	0.64	-10.5	14.5
0	0	0	0	300.2	110.2	33.1	2.11	2150	2010	0.67	0.62	-9.9	22.9
299.3	27.5	300.4	66.1	0	0	28.1	1.85	2100	1960	0.68	0.63	-9.0	19.7
299.3	25.4	0	0	300.1	110.5	40.8	2.58	2110	2030	0.65	0.62	-12.7	26.0
0	0	305.1	63.1	300.0	110.6	52.4	3.30	2102	2002	0.65	0.61	-12.8	31.9
299.1	25.7	304.6	62.4	300.0	110.0	60.0	3.74	2070	1970	0.63	0.60	-14.4	36.2
298.9	32.9	0	0	0	0	9.84	0.66	2040	1910	0.67	0.62	-9.8	7.5
0	0	288.1	79.84	0	0	23.00	1.48	1950	1820	0.62	0.57	-9.6	17.0
0	0	0	0	299.3	137.5	41.2	2.55	2150	2010	0.65	0.61	-9.9	27.2
298.4	33.6	300.1	78.6	298.1	138.5	74.9	4.64	2130	2020	0.65	0.61	-11.4	42.2

Table 5. 400 V throttle table for the X3 performance measurements.

$V_{d,I}$ V	$I_{d,I}$ A	$V_{d,M}$ V	$I_{d,M}$ A	$V_{d,O}$ V	$I_{d,O}$ A	$P_{d,t}$ kW	T N	$I_{sp,a}$ s	$I_{sp,t}$ s	η_a –	η_t –	V_{cg} V	p_b μTorr
400.4	16.2	0	0	0	0	6.5	0.39	2190	2050	0.64	0.59	-13.7	4.3
0	0	400.1	39.8	0	0	15.9	0.93	2210	2060	0.63	0.59	-12.6	9.7
0	0	0	0	400.0	68.9	27.6	1.58	2360	2200	0.66	0.61	-10.7	15.9
400.2	16.9	0	0	399.7	68.8	34.2	1.94	2380	2220	0.66	0.61	-10.1	18.5
0	0	394.8	38.9	399.6	69.7	43.2	2.45	2350	2200	0.65	0.61	-10.4	23.0
400.1	16.5	394.4	39.3	399.6	68.8	49.5	2.77	2310	2160	0.63	0.59	-9.8	25.6
399.77	26.4	0	0	0	0	10.6	0.61	2290	2140	0.65	0.60	-11.48	6.3
0	0	399.5	63.7	0	0	25.5	1.49	2360	2210	0.68	0.63	-10.6	14.1
0	0	0	0	399.1	106.9	42.7	2.40	2450	2330	0.68	0.64	-10.9	22.0
399.6	25.9	399.5	63.4	0	0	35.7	2.07	2420	2270	0.69	0.64	-8.8	19.0
399.7	25.0	0	0	399.8	109.0	53.6	2.98	2450	2290	0.67	0.62	-9.7	26.6
0	0	393.0	64.6	399.7	109.8	69.3	3.94	2460	2300	0.69	0.64	-10.8	32.6
399.5	25.7	401.0	64.1	399.6	109.9	79.9	4.49	2440	2240	0.67	0.61	-10.8	37.0
398.6	33.8	402.7	76.1	398.2	136.9	98.6	5.42	2470	2340	0.67	0.63	-11.3	41.8

Table 6. 500 V throttle table for the X3 performance measurements.

$V_{d,I}$ V	$I_{d,I}$ A	$V_{d,M}$ V	$I_{d,M}$ A	$V_{d,O}$ V	$I_{d,O}$ A	$P_{d,t}$ kW	T N	$I_{sp,a}$ s	$I_{sp,t}$ s	η_a –	η_t –	V_{cg} V	p_b μTorr
500.7	16.5	0	0	0	0	8.2	0.43	2460	2300	0.64	0.59	-12.9	4.4
0	0	500.9	39.3	0	0	19.7	1.08	2590	2420	0.70	0.64	-12.9	9.9
0	0	0	0	500.4	67.4	33.7	1.77	2770	2580	0.71	0.66	-12.2	14.7
500.5	17.0	500.6	39.1	0	0	38.0	1.37	2450	2290	0.59	0.54	-9.1	12.6
500.4	16.8	0	0	500.3	67.5	42.2	2.19	2740	2560	0.70	0.64	-9.9	17.8
0	0	508.6	37.3	500.6	68.8	53.4	2.62	2790	2590	0.67	0.61	-12.1	20.7
500.2	18.0	499.2	38.1	500.6	68.6	62.4	3.28	2760	2580	0.71	0.66	-10.2	25.1
500.1	26.1	0	0	0	0	13.1	0.70	2680	2500	0.71	0.66	-10.9	6.2
0	0	500.4	62.3	0	0	31.2	1.69	2710	2530	0.72	0.67	-10.8	14.0
0	0	0	0	499.6	109.5	54.7	2.77	2840	2650	0.70	0.65	-10.4	21.9
499.9	26.3	499.8	63.7	0	0	45.0	2.34	2720	2540	0.69	0.64	-8.7	18.5
499.8	26.2	0	0	500.7	109.2	67.8	3.38	2800	2610	0.68	0.63	-9.6	25.3
0	0	504.3	63.8	499.4	110.0	87.1	4.34	2740	2560	0.67	0.62	-10.9	32.2
499.4	28.2	505.3	63.2	499.6	110.1	101.0	5.03	2750	2570	0.67	0.63	-10.3	35.9

Acknowledgments

Scott J. Hall and Matthew J. Baird are supported by NASA Space Technology Research Fellowships under grant numbers NNX14AL67H and NNX16AM96H. A portion of the work described here was performed as a part of NASA's NextSTEP program under grant number NNH16CP17C. The plasma diagnostics were funded by a Michigan Institute of Plasma Science and Engineering Graduate Student Fellowship. The authors would like to acknowledge a number of personnel at NASA Glenn Research Center who contributed to this work, including Eric Pencil, Luis Piñero, Wensheng Huang, Taylor Seablom, Chad Joppeck, Richard Senyitko, Jim Zakany, Nick Lalli, Jim Zologowski, Kevin Blake, Josh Gibson, Dave Yendriga, Larry Hambly, and George Jacynycz. The authors gratefully acknowledge Dan M. Goebel at NASA JPL for providing the cathode used in this experiment, Sarah E. Cusson at the University of Michigan for magnetic field optimization work, and Joshua M. Woods at the University of Michigan for assistance with plasma diagnostics.

References

[1]Brown, D. L., Beal, B. E., and Haas, J. M., "Air Force Research Laboratory High Power Electric Propulsion Technology Development," *2010 IEEE Aerospace Conference*, Big Sky, MT, March 2010.

[2]Oleson, S., "Advanced electric propulsion for space solar power satellites," Vol. AIAA-99-2872, American Institute of Aeronautics and Astronautics, Los Angeles, CA, 1999.

[3]Woodcock, G. and Wingo, D., "Flight Mechanics and Control Requirements for a Modular Solar Electric Tug Operating in Earth-Moon Space," *AIP Conference Proceedings*, Vol. 813, AIP, 2006, pp. 982–991.

[4]Brophy, J. R., Gershman, R., Strange, N., Landau, D., Merrill, R., and Kerslake, T., "300-kW Solar Electric Propulsion System Configuration for Human Exploration of Near-Earth Asteroids," *47th Joint Propulsion Conference*, Vol. 5514, AIAA, San Diego, CA, Aug. 2011.

[5]Myers, R. and Carpenter, C., "High power solar electric propulsion for human space exploration architectures," *32nd International Electric Propulsion Conference*, 2011, pp. 2011–261.

[6]Myers, R. M., Joyner, C. R., Cassady, R. J., Overton, S., Kokan, T., Horton, J., and Hoskins, W. A., "Affordable Exploration Architectures Using the Space Launch System and High Power Solar Electric Propulsion," *34th International Electric Propulsion Conference*, Electric Rocket Propulsion Society, Kobe, Japan, July 2015.

[7]Strange, N., Merrill, R., Landau, D., Drake, B., Brophy, J., and Hofer, R., "Human missions to phobos and deimos using combined chemical and solar electric propulsion," *47th AIAA Joint Propulsion Conference*, 2011.

[8]Hofer, R. R. and Randolph, T. M., "Mass and cost model for selecting thruster size in electric propulsion systems," *Journal of Propulsion and Power*, Vol. 29, No. 1, 2012, pp. 166–177.

[9]Patterson, M. J. and Benson, S. W., *NEXT ion propulsion system development status and performance*, National Aeronautics and Space Administration, Glenn Research Center, 2008.

[10]Kamhawi, H., Haag, T. W., Jacobson, D. T., and Manzella, D. H., "Performance Evaluation of the NASA-300M 20 kW Hall Effect Thruster," *47th AIAA Joint Propulsion Conference*, American Institute of Aeronautics and Astronautics, San Diego, CA, Aug. 2011.

[11]Manzella, D., *Scaling Hall Thrusters to High Power*, Ph.D. thesis, Stanford University, Stanford, CA, 2005.

[12]Manzella, D., Jankovsky, R., and Hofer, R., "Laboratory Model 50 kW Hall Thruster," *38th AIAA Joint Propulsion Conference*, American Institute of Aeronautics and Astronautics, Indianapolis, IN, July 2002.

[13]Jacobson, D. T. and Manzella, D. H., "50 kW Class Krypton Hall thruster Performance," *39th Joint Propulsion Conference*, 20-23 July 2003, 2003.

[14]Soulas, G., Haag, T., Herman, D., and Huang, W., "Performance Test Results of the NASA-457M v2 Hall Thruster," *48th AIAA Joint Propulsion Conference*, American Institute of Aeronautics and Astronautics, Atlanta, GA, Aug. 2012.

[15]Peterson, P. Y., Jacobson, D. T., Manzella, D. H., and John, J. W., "The performance and wear characterization of a high-power high-Isp NASA Hall thruster," *41st Joint Propulsion Conference*, American Institute of Aeronautics and Astronautics, 2005.

[16]Spores, R., Monheiser, J., Dempsey, B., Wade, D., Creel, K., Jacobson, D., and Drummond, G., "A Solar Electric Propulsion Cargo Vehicle to Support NASA Lunar Exploration Program," Princeton, NJ, 2005.

[17]Brown, D. L., Haas, J. M., Peterson, P. Y., and Kirtley, D. E., "Development of High-Power Electric Propulsion Technology for Near-Term and Mid-Term Space Power," *57th Joint Army Navy NASA Air Force Propulsion Meeting*, Colorado Springs, CO, May 2010.

[18]Hall, S. J., Jorns, B. A., Gallimore, A. D., and Hofer, R. R., "Expanded Thruster Mass Model Incorporating Nested Hall Thrusters," *53rd AIAA/SAE/ASEE Joint Propulsion Conference*, 2017, p. 4729.

[19]Szabo, J., Pote, B., Hruby, V., Byrne, L., Tedrake, R., Kolencik, G., Kamhawi, H., and Haag, T. W., "A commercial one Newton Hall effect thruster for high power in-space missions," *AIAA Paper*, Vol. 6152, 2011.

[20]Liang, R., *The Combination of Two Concentric Discharge Channels into a Nested Hall-Effect Thruster*, Ph.D. thesis, University of Michigan, Ann Arbor, MI, 2013.

[21]Florenz, R. E., Gallimore, A. D., and Peterson, P., "Developmental Status of a 100-kW Class Laboratory Nested Channel Hall Thruster," *32nd International Electric Propulsion Conference*, Wiesbaden, Germany, Sept. 2011.

[22]Florenz, R. E., Hall, S. J., Gallimore, A. D., Kamhawi, H., Griffiths, C. M., Brown, D. L., Hofer, R. R., and Polk, J. E., "First Firing of a 100-kW Nested-channel Hall Thruster," *33rd International Electric Propulsion Conference*, Washington D.C., Oct. 2013.

[23]Florenz, R. E., *The X3 100-kW Class Nested-Channel Hall Thruster: Motivation, Implementation, and Initial Performance*, Ph.D. thesis, University of Michigan, Ann Arbor, MI, 2013.

[24]Hall, S. J., Florenz, R. E., Gallimore, A. D., Kamhawi, H., Brown, D. L., Polk, J. E., Goebel, D., and Hofer, R. R., "Implementation and Initial Validation of a 100-kW Class Nested-channel Hall Thruster," *50th AIAA Joint Propulsion Conference*, American Institute of Aeronautics and Astronautics, Cleveland, OH, July 2014.

[25]Hall, S. J., Cusson, S. E., and Gallimore, A. D., "30-kW Performance of a 100-kW Class Nested-channel Hall Thruster," *34th International Electric Propulsion Conference*, Kobe-Hyogo, Japan, July 2015.

[26]McDonald, M. S., Sekerak, M. J., Gallimore, A. D., and Hofer, R. R., "Plasma Oscillation Effects on Nested Hall Thruster Operation and Stability," *2013 IEEE Aerospace Conference*, IEEE, Big Sky, MT, 2013, pp. 1–12.

[27]NASA, "Next Space Technologies for Exploration Partnerships Broad Agency Announcement," Oct. 2014.

[28]Jackson, J., Allen, M., Myers, R., Hoskins, A., Soendker, E., Welander, B., Tolentino, A., Hablitzel, S., Hall, S. J., Jorns, B. A., Gallimore, A. D., Hofer, R. R., and Pencil, E., "100-kW Nested Hall Thruster System Development," Vol. IEPC-2017-219, Atlanta, GA, Oct. 2017.

[29]Goebel, D. M. and Chu, E., "High-Current Lanthanum Hexaboride Hollow Cathode for High-Power Hall Thrusters," *Journal of Propulsion and Power*, Vol. 30, No. 1, 2014, pp. 35–40.

[30]Hall, S. J., Florenz, R. E., Gallimore, A. D., Kamhawi, H., Peterson, P. Y., Brown, D. L., Hofer, R. R., and Polk, J. E., "Design Details of a 100-kW Class Nested-channel Hall Thruster," *62nd Joint Army Navy NASA Air Force Propulsion Meeting*, Nashville, TN, June 2015.

[31]Kamhawi, H. and VanNoord, J., "Development and Testing of High Current Hollow Cathodes for High Power Hall Thrusters," *48th Joint Propulsion Conference*, Vol. 4080, AIAA, Atlanta, GA, 2012.

[32]Thomas, R. E., Kamhawi, H., and Williams, Jr., G. J., "High Current Hollow Cathode Plasma Plume Measurements," *33rd International Electric Propulsion Conference*, Washington D.C., Oct. 2013.

[33]Chu, E., Goebel, D. M., and Wirz, R. E., "Reduction of Energetic Ion Production in Hollow Cathodes by External Gas Injection," *Journal of Propulsion and Power*, Vol. 29, No. 5, 2013, pp. 1155–1163.

[34]Peterson, P. Y., Kamhawi, H., Huang, W., Williams, G., Gilland, J. H., Yim, J., Hofer, R. R., and Herman, D. A., "NASA HERMeS Hall Thruster Electrical Configuration Characterization," *52nd AIAA/SAE/ASEE Joint Propulsion Conference*, 2016, p. 5027.

[35]Yim, J. and Burt, J. M., "Characterization of Vacuum Facility Background Gas Through Simulation and Considerations for Electric Propulsion Ground Testing," American Institute of Aeronautics and Astronautics, Orlando, FL, July 2015.

[36]Kamhawi, H., Haag, T., Huang, W., Herman, D. A., Thomas, R., Shastry, R., Yim, J., Chang, L., Clayman, L., Verhey, T., and others, "Performance Characterization of the Solar Electric Propulsion Technology Demonstration Mission 12.5-kW Hall Thruster," *34th International Electric Propulsion Conference, IEPC-2015-007, Kobe, Japan*, 2015.

[37]Kamhawi, H., Haag, T., Huang, W., Yim, J., Herman, D. A., Peterson, P. Y., Williams, G., Gilland, J., Hofer, R. R., and Mikellides, I. G., "Performance, Facility Pressure Effects, and Stability Characterization Tests of NASAs 12.5-kW Hall Effect Rocket with Magnetic Shielding Thruster," *52nd AIAA/SAE/ASEE Joint Propulsion Conference*, American Institute of Aeronautics and Astronautics, 2016, DOI: 10.2514/6.2016-4826.

[38]Hall, S. J., Gallimore, A. D., and Viges, E., "Thrust Stand for Very-High-Power Hall Thrusters," *63rd Joint Army Navy NASA Air Force Propulsion Meeting*, Phoenix, AZ, Dec. 2016.

[39]Haag, T., "Thrust Stand for High-Powered Electric Propulsion Devices," *Review of Scientific Instruments*, Vol. 62, No. 1186, 1991.

[40]Xu, K. G. and Walker, M. L., "High-power, null-type, inverted pendulum thrust stand," *Review of Scientific Instruments*, Vol. 80, No. 5, 2009, pp. 055103.

[41]Polk, J. E., Pancotti, A., Haag, T., King, S., Walker, M., Blakely, J., and Ziemer, J., "Recommended Practice for Thrust Measurement in Electric Propulsion Testing," *Journal of Propulsion and Power*, Vol. 33, No. 3, 2017, pp. 539–555.

[42]Huang, W., Shastry, R., Soulas, G. C., and Kamhawi, H., "Farfield Plume Measurement and Analysis on the NASA-300M and NASA-300MS," *33rd International Electric Propulsion Conference*, Washington D.C., 2013.

[43]Huang, W., Kamhawi, H., and Haag, T., "Facility Effect Characterization Test of NASAs HERMeS Hall Thruster," *52nd AIAA/SAE/ASEE Joint Propulsion Conference*, 2016, p. 4828.

[44]Cusson, S. E., Hall, S. J., Hofer, R. R., Jorns, B. A., and Gallimore, A. D., "The Impact of Magnetic Field Coupling Between Channels in a Nested Hall Thruster," Vol. IEPC-2017-507, Atlanta, GA, 2017.

[45]Hofer, R. R., Jankovsky, R. S., and Gallimore, A. D., "High-specific impulse Hall thrusters, part 1: Influence of current density and magnetic field," *Journal of Propulsion and Power*, Vol. 22, No. 4, 2006, pp. 721–731.

[46]Hofer, R. R. and Gallimore, A. D., "High-Specific Impulse Hall Thrusters, Part 2: Efficiency Analysis," *Journal of Propulsion and Power*, Vol. 22, No. 4, 2006, pp. 732–740.

[47]Georgin, M. P., Dhaliwal, V., and Gallimore, A., "Investigation of Channel Interactions in a Nested Hall Thruster Part I: Acceleration Region Velocimetry," *52nd AIAA/SAE/ASEE Joint Propulsion Conference*, Salt Lake City, UT, July 2016, p. 5030.

[48]Cusson, S. E., Dale, E. T., and Gallimore, A., "Investigation of Channel Interactions in a Nested Hall Thruster Part II: Probes and Performance," *52nd AIAA/SAE/ASEE Joint Propulsion Conference*, Salt Lake City, UT, July 2016, p. 5029.

[49]Beal, B. E., Gallimore, A. D., and Hargus, W. A., "Effects of Cathode Configuration on Hall Thruster Cluster Plume Properties," *Journal of Propulsion and Power*, Vol. 23, No. 4, 2007, pp. 836–844.

[50]Sekerak, M. J., Gallimore, A. D., Brown, D. L., Hofer, R. R., and Polk, J. E., "Mode Transitions in Hall-Effect Thrusters Induced by Variable Magnetic Field Strength," *AIAA Journal of Propulsion and Power*, March 2016.

[51]McDonald, M. S. and Gallimore, A. D., "Rotating spoke instabilities in Hall thrusters," *IEEE Transactions on Plasma Science*, Vol. 39, No. 11, 2011, pp. 2952–2953.

[52]Ellison, C. L., Raitses, Y., and Fisch, N. J., "Cross-field electron transport induced by a rotating spoke in a cylindrical Hall thruster," *Physics of Plasmas*, Vol. 19, No. 1, 2012, pp. 013503.

[53]Goebel, D. M., Jameson, K. K., Katz, I., and Mikellides, I. G., "Potential fluctuations and energetic ion production in hollow cathode discharges," *Physics of Plasmas*, Vol. 14, No. 10, 2007, pp. 103508.

[54]Choueiri, E. Y., "Plasma oscillations in Hall thrusters," *Physics of Plasmas*, Vol. 8, No. 4, 2001, pp. 1411–1426.

[55]Sommerville, J. D. and King, L. B., "Effect of cathode position on Hall-effect thruster performance and cathode coupling voltage," *Proceedings of the 43rd AIAA/ASME/SAE/ASEE Joint Propulsion Conference, AIAA-2007-5174, Cincinnati, OH*, 2007.

[56]Jameson, K. K., Goebel, D. M., Hofer, R. R., and Watkins, R. M., "Cathode coupling in Hall thrusters," *30th International Electric Propulsion Conference*, 2007, pp. 2007–278.

[57]McDonald, M. S. and Gallimore, A. D., "Cathode position and orientation effects on cathode coupling in a 6-kW Hall thruster," *31st International Electric Propulsion Conference*, Vol. 113, 2009.

[58]Brown, D. L. and Gallimore, A. D., "Investigation of low discharge voltage hall thruster operating modes and ionization processes," Ann Arbor, MI, 2009.

[59]Jorns, B. A. and Hofer, R. R., "Plasma oscillations in a 6-kW magnetically shielded Hall thruster," *Physics of Plasmas*, Vol. 21, No. 5, 2014, pp. 053512.